NMR Solution Structure of a Synthetic Troponin C Heterodimeric Domain[†,‡]

Gary S. Shaw[§] and Brian D. Sykes*[,||]

Department of Biochemistry & McLaughlin Macromolecular Structure Facility, The University of Western Ontario, London, Ontario, Canada, N6A 5C1, and Department of Biochemistry and MRC Group in Protein Structure & Function, University of Alberta, Edmonton, Alberta T6G 2H7, Canada

Received November 27, 1995; Revised Manuscript Received April 4, 1996[⊗]

ABSTRACT: The C-terminal domain from the muscle protein troponin C (TnC) comprises two helix−loop−helix calcium-binding sites (residues 90−162). The assembly of these two sites is governed by calcium binding enabling a synthetic C-terminal domain to be preferentially and stoichiometrically assembled from two synthetic peptides (residues 93−126, SCIII, and 129−162, SCIV) in the presence of calcium only. It is therefore of great interest to know how closely the structure of this heterodimeric domain is to the intact protein domain. Analysis of such a structure has important implications in protein engineering and in understanding the stability of calcium-binding proteins in terms of biological function. The solution structure of this heterodimeric protein was determined by ^{1}H NMR spectroscopy using 802 NOE derived distance restraints and 23 ϕ and 22 χ_1 angle restraints. Distance geometry−simulated annealing calculations yielded a family of 42 converged structures (rmsd 0.86 ± 0.17 Å) showing an arrangement of four α-helices similar in fold to the C-terminal of troponin C. The dimer interface has several important interactions between helix pairs E/H and F/G responsible for the association of the two peptides. However, neither the peptide complex nor the solution NMR structure of TnC pack as tightly as that observed in the TnC X-ray structure. The interhelical distance between the F/G helix is about 1.4 Å greater in solution than in the crystal. A comparison of the exposed surface area of the hydrophobic residues in the SCIII/SCIV heterodimer revealed that residues I104, Y112, and I121 are more exposed than in the previously determined solution structure of the SCIII homodimer. These residues are important for the interaction with the inhibitory region of TnI and provide evidence for their involvement in the regulation of muscle contraction.

An important class of metal-ion binding proteins is the "EF-hand" or "helix−loop−helix" family of calcium-binding proteins. Members of this family include the muscle contractile protein troponin C, the multifunctional protein calmodulin, the glial protein S100b, and the photoreceptor protein recoverin. These calcium-binding proteins have several key structural features which centre around the helix−loop−helix motif (Kretsinger & Nockolds, 1973), a contiguous stretch of about 30 amino acids, which forms the calcium-binding site. The architecture of each calcium-binding site can further be divided into a 12-residue loop, where calcium is coordinated, and two flanking 9−14 residue α-helices. Sequence analysis of over 100 calcium-binding proteins, including 276 calcium-binding loops, has identified that EF-hand calcium-binding proteins are always composed of two to eight copies of this motif (Marsden et al., 1989). In all cases studied to date, it has further been observed that these calcium-binding sites are paired to form a two-site domain. X-ray crystallographic studies have revealed that the calcium-binding site proteins calbindin D_{9k} (Szebenyi & Moffat, 1986) and parvalbumin (Declercq et al., 1988; Kretsinger & Nockolds, 1973; Swain et al., 1989) which have two calcium-binding sites form a single two-site domain. Other calcium-binding proteins such as troponin-C (Herzberg & James, 1988; Satyshur et al., 1988, 1994), calmodulin (Babu et al., 1988), and recoverin (Flaherty et al., 1993) have four calcium-binding sites and form two two-site domains, although some interactions exist between these.

An important feature of the two-site calcium-binding domains is that a pseudo-two-fold symmetry exists within a pair of helix−loop−helix calcium-binding sites. The centroid of this symmetry is a short, three-residue, antiparallel β-sheet which is formed between residues 7−9 of each calcium-binding loop. In the C-terminal of troponin C, this β-sheet is comprised of residues F112−D114 of site III and R148−D150 of site IV. A second feature of the symmetry is the arrangement of the α-helices in the two sites. Each helix is approximately perpendicular to both its partner helix in the same site, and its partner's symmetrically related helix in the second site (Strynadka & James, 1989). For example, site III in the C-terminal of troponin C is comprised of helices E and F, which are roughly perpendicular (∼110°) to each other. Similar interhelical angles exist between helix E and helix H (∼116°) and helix F with helix G (∼120°). This crossing of helices results in significant hydrophobic interactions at the interfaces of these helices and has been suggested to contribute to the considerable stability of EF-hand proteins.

Synthetic peptides containing single calcium-binding sites are important for studying calcium-binding proteins. An

[†] This work was supported by grants from the Medical Research Council of Canada and a fellowship (G.S.S.) from the Alberta Heritage Foundation for Medical Research.

[‡] The coordinates have been deposited in the Brookhaven Protein Data Bank (File: 1PON). Coordinates for the 42 DGII structures and the restraint file used to generate the structures have been deposited with the Protein Data Bank (accession codes: coordinates, 1PON; restraints, R1PONMR).

* Author to whom correspondence should be addressed.

[§] The University of Western Ontario.

[||] University of Alberta.

[⊗] Abstract published in *Advance ACS Abstracts,* May 15, 1996.

S0006-2960(95)02800-5 CCC: $12.00

understanding of the calcium-binding properties and stabilities of these EF-hand proteins can be obtained from investigations using two-site dimers in an effort to design calcium-binding proteins. In troponin C, homodimers comprised of either two site III peptides (Shaw et al., 1990) or a heterodimer containing site III and site IV peptides can be formed upon calcium binding (Shaw et al., 1992a). This finding may be a general observation for EF-hand calcium-binding proteins as similar two-site peptide associations have now been determined sites I and II in calbindin D_{9k} (Finn et al., 1992; Linse et al., 1993) and the N-terminal of the *Nereis* sarcoplasmic calcium-binding protein (Durussel et al., 1993). More recently, it has been shown that a heterodimeric site III−site IV complex is preferentially formed compared to the individual homodimers in the presence of calcium (Shaw et al., 1992a). This SCIII/SCIV[1] heterodimer binds two equivalents of calcium with similar affinities (K_d 2−3 μM) in contrast to the SCIII homodimer (K_{d1} 3 μM, K_{d2} 1 mM) and the weak calcium-binding SCIV homodimer (K_d > 260 μM) (Shaw et al., 1991, 1992c). These observations suggest that there is an important relationship between the calcium affinities and the composition of the calcium-binding sites (Monera et al., 1992; Shaw et al., 1994). In the present work we have determined the solution structure of the SCIII/SCIV heterodimer using distance restraints obtained from two-dimensional NOESY spectra and distance geometry−simulated annealing (DGII). The data utilize unambiguous assignment of resonances and NOEs at the interface of the SCIII/SCIV heterodimer which are responsible for the association of the two peptides. We have analyzed this structure and compared it to the NMR solution structures of the III/III homodimer and TnC and the X-ray structure of TnC to propose a basis for the biologically active form of TnC and its interaction with the inhibitory region of TnI.

EXPERIMENTAL PROCEDURES

Sample Preparation. Synthetic 34-residue peptides comprising residues 93−126 (SCIII) and 129−162 (SCIV) of chicken skeletal troponin C (SCIII) were synthesized using an Applied Biosystems Peptide Synthesizer (Model 430A). Purification was accomplished by reversed-phase HPLC using a C8 semipreparative column, and the peptide composition was verified by amino acid analysis and mass spectrometry. Details of the synthesis and purification of both peptides have been published previously (Shaw et al., 1991).

NMR Spectroscopy. Purified, freeze-dried SCIII (13.34 mg) and SCIV (13.96 mg) peptides were dissolved separately in 1.0 mL of D_2O which was 25 mM KCl, at pH 7.19 and 7.41, respectively. From each solution, 2 μL was diluted to 25 μL with 0.05% TFA in H_2O, and 10 μL of each was co-injected onto a C18 analytical column and analyzed by reversed-phase HPLC as previously described (Shaw et al., 1991). The peaks corresponding to SCIII and SCIV were integrated to determine the relative proportions of SCIII and SCIV in the mixture. The stock SCIII and SCIV peptide solutions were also assayed by quantitative amino acid analysis to determine the absolute peptide concentrations of each. Based on these analyses, 490 μL of the stock 1 mL sample of SCIV was added to the remainder of the SCIII stock solution (960 μL), and the composite sample was lyophilized. The peptide sample was dissolved in 425 μL of deionized H_2O and 75 μL of D_2O and 5.1 μL of a stock 980.4 mM $CaCl_2$ solution in D_2O added. This resulted in a final SCIII/SCIV heterodimer concentration of 2.2 mM in 85% H_2O/15% D_2O, 9.9 mM $CaCl_2$, and 75 mM KCl at pH 7.19 which was used for all NMR experiments obtained in H_2O. Following the acquisition of these data, the peptide solution was lyophilized and the resulting material redissolved in 99.96% D_2O.

All NMR spectra were obtained on a Varian Unity 600 spectrometer in the phase-sensitive mode. Sequence-specific assignments were carried out at 30 °C; however, spectra were also recorded at 15 °C to resolve overlapping amide resonances. In all experiments, water suppression was accomplished by a weak presaturation pulse of 2 s. duration. For each temperature and solvent conditions DQF-COSY (Piantini et al., 1982), TOCSY (Bax & Davis, 1985) and NOESY experiments were acquired. TOCSY experiments were collected using MLEV-17 spin lock mixing periods of 30 and 50 ms. Typical data sets were comprised of 32 or 48 transients for each of 320 or 512 t_1 increments. Spectral widths of 8000 Hz in 85% H_2O/15% D_2O and 6000 Hz in D_2O were used. DQF-COSY spectra were processed using a sine-bell weighting function yielding final digital resolutions of 3.9 Hz/point (H_2O) or 2.9 Hz/point (D_2O) in F_1 and F_2. NOESY spectra were collected by the hypercomplex method (States et al., 1982) for mixing times (τ_m) of 50, 150, and 300 ms in H_2O and 150 ms in D_2O solution. In each case a random delay of ±15 ms (±20 ms for $\tau_m = 300$ ms) was employed to suppress zero-quantum coherence. Spectra were processed using a $\pi/8$ shifted sine-bell and baseline corrected in F_2.

Data Analysis. Spin−spin coupling constant information was obtained from DQF-COSY spectra in H_2O ($^3J_{NH\alpha}$) and D_2O ($^3J_{\alpha\beta}$). Data was zero filled in F_2 to final digital resolutions of 0.98 Hz/point (H_2O) and 0.73 Hz/point (D_2O). Traces of each resolved cross peak were taken along F_2 and the two antiphase components fitted using an in-house iterative curve fitting program written by Robert Boyko at the University of Alberta. Stereospecific assignments (Wagner et al., 1987) for several prochiral methylene centers were obtained using the cross peak patterns for $^3J_{\alpha\beta}$ from DQF-COSY spectra and the intraresidue NOEs taken from NOESY spectra with short mixing times ($\tau_m = 50$ ms). This yielded stereospecific assignments for the β protons of L98, N100, F102, F105, D106, D114, D133, D136, L137, D140, D142, N144, N145, D150, F151, F154, and L155.

Structure Calculations. Cross peaks were assigned from 300 ms NOESY spectra and the NOE intensities were measured by taking the volume integral of each crosspeak from 50 ms NOESY spectra. Intensities were calibrated using the δCH to ϵCH distance of 2.46 Å for the corresponding well resolved cross peaks of F102 and F151. The integrated intensities were divided into four classes of distances with bounds of 1.8−2.5, 1.8−3.0, 1.8−4.0, and 1.8−5.0 Å based on a similar approach used for the

[1] Abbreviations: SCIII, synthetic site III troponin C peptide (residues 93−126); SCIV, synthetic site IV troponin C peptide (residues 129−162); TnC, troponin C; TR_1C, N-terminal domain of troponin C; cTnC, cardiac troponin C; helix E, residues 95−105 in TnC; helix F, residues 115−124 in TnC; helix G, residues 131−141 in TnC; helix H, residues 151−157 in TnC; TFA, trifluoroacetic acid; DQF-COSY, double quantum filtered correlation spectroscopy; TOCSY, total correlation spectroscopy; NOESY, nuclear Overhauser enhancement spectroscopy; RMSD, root mean square deviation.

N-terminal domain of TnC (Findlay et al., 1994) and which was found to be particularly useful for this α-helical protein. For stereospecifically assigned protons, distance restraints were imposed on the appropriate *R* and/or *S* proton as assigned. For resolvable methylene protons which were not stereospecifically assigned, and where an NOE was observed to both protons, the higher of the upper bounds was applied to both protons (Hyberts et al., 1992). A similar approach was applied to the δCH_3 groups of leucine and γCH_3 groups of valine residues. For all other methylene and methyl groups, standard pseudoatom replacements and distance corrections were used. Methyl groups also had an additional 0.5 Å added to the upper bounds to account for the higher observed intensity of these residues.

Coupling constant information was used to impose dihedral angle restraints. For the polypeptide backbone, phi (ϕ) was restricted to $-90° \leq \phi \leq 40°$ where $^3J_{NH\alpha} < 6$ Hz and $150° \leq \phi \leq -150°$ when $^3J_{NH\alpha} > 10$ Hz. Cross peaks which were either absent or very weak in DQF-COSY spectra were assumed to arise from severe cancelation of antiphase components having $^3J_{NH\alpha} < 6$ Hz. Residues which could not unambiguously be assigned to either class were restricted to the allowed region of Ramachandran space where $-180° \leq \phi \leq 0°$. Two residues (A108 and N145) were classified to have $40° \leq \phi \leq 90°$ based on the presence of a very strong intraresidue NHα NOE (Kline et al., 1988). Side-chain angular restraints were derived from DQF-COSY spectra and stereospecifically assigned protons for χ_1. This resulted in 11 residues where $-90 \leq \chi_1 \leq -30$, 8 residues where $150 \leq \chi_1 \leq -150$, and 3 residues where $30 \leq \chi_1 \leq 90$. Hydrogen bond distance restraints were introduced only in stretches of amino acids where $d_{\alpha N}(i,i+3)$ and/or $d_{\alpha\beta}(i,i+3)$ NOEs and $d_{NN}(i,i+1)$ NOEs were evident and where initial structure calculations resulted in α-helix formation. The exceptions to this were two hydrogen bonds which were introduced between I113 and I149. These restraints were rationalized from the observation of a $d_{\alpha\alpha}$ NOE between Y112 αCH and D150 αCH, the downfield shift of the αCH for Y112, I113, D114, R148, I149, and D150, and the numerous NOEs between the side chains of these residues. Initial structure calculations without this hydrogen bond also showed that the NH and C═O of I113 were in close proximity with I149 C═O and NH, respectively. In all cases, generic hydrogen bonds were introduced with 2.7−3.0 Å boundaries between the amide nitrogen and carbonyl oxygen and 1.8−2.0 Å between the amide proton and carbonyl oxygen (Akke et al., 1992). Calcium ions, or restraints to confine calcium-binding loops to a particular conformation, were not included in these calculations.

Structure calculations were performed using DGII (Bio-Sym Technologies, v 2.2.0) using a total of 802 NOE derived distance restraints, 84 dihedral restraints, and 50 hydrogen-bonding restraints. Full matrix distance bounds were computed for all atoms using tetragonal inequalities for sequential residues. Embedding of coordinates was done in four dimensions following metrization (prospective). Larger distance bounds were weighed to a lesser extent using the *range and average* option during majorization. Distance bounds were optimized over 10 000 steps (0.2 ps) of simulated annealing (maximum temperature 2100 K) where an error function including distance bound violations was minimized. Structures which converged to an error of <0.3 were subjected to 250 steps conjugate gradient minimization. Structure quality assessment was done using the Procheck (v 3.2) and Procheck_NMR suite of programs (Laskowski et al., 1993). Structural calculations were repeated using the program X-PLOR and the identical restraints for 30 structures (data not shown). Interhelical angles and distances were calculated using a program written by Kyoko Yap and Mitsuhiko Ikura (University of Toronto).

RESULTS AND DISCUSSION

Sequence-Specific Assignment and Secondary Structure. The complete ^1H assignment of the SCIII/SCIV heterodimer was carried through the identification of spin systems from TOCSY spectra, measured with spin-locking times of 30 and 50 ms, and DQF-COSY spectra measured at both 30 and 15 °C as has been described earlier for the SCIII homodimer (Shaw et al., 1992b). The assignment of the heterodimer was facilitated through the excellent resolution in the α,β region for AMX spin systems where 16 out of 21 AMX type amino acids could be categorized from the analysis of these two spectra. For TOCSY spectra, longer side chain amino acids such as R and K were assigned easily from "reverse" correlations from either the δ or ϵ protons, respectively. Correlations were also completed using the αCH resonances in addition to conventional NH correlations as done previously for the SCIII homodimer (Shaw et al., 1992b). In addition, the large separation in chemical shift between β protons of residues which chelate the calcium ion (frequently >0.5 ppm) was used to identify these residues compared to other nonligating AMX spin system residues (Shaw et al., 1992b). Sequential assignment of these spin systems was accomplished using several NOESY spectra with mixing times ranging from 50 to 300 ms following the established methods of Wüthrich (1985). The complete assignment of the SCIII/SCIV heterodimer can be found in the Supporting Information.

Upon complete sequential assignment of the SCIII/SCIV heterodimer, medium-range interactions in the NOESY spectra were identified in order to establish the secondary structures of the peptides. Figure 1 shows the NH/NH region of the 150 ms NOESY spectrum illustrating the large number of connectivities between adjacent amide protons. Four distinct stretches of NH/NH connectivities were identified in this spectrum, consistent with four regular and separated α-helices in the complex. For example, Figure 1 shows strong NH/NH interactions for residues E96−R103, E117−R123, I134−D142, and F151−M157. In addition, several NH/NH interactions were noted for residues in the calcium-binding loops of the dimer. Figure 1 shows four of these NOEs resulting from interactions between amide proton pairs of D110,G111; G111,Y112; D146 and G147, R148. Both of these observations are remarkably similar to those noted for the individual site III (Shaw et al., 1992b) and site IV (Kay et al., 1991) homodimers and in turkey skeletal TnC (Slupsky et al., 1995; Slupsky & Sykes, 1995).

Upon examination of the 50 and 150 ms NOESY spectra, the secondary structures for the SCIII/SCIV heterodimer peptides was determined. As summarized in Figure 2, sequential assignment was supported by several $d_{\alpha N}(i,i+1)$ and $d_{\beta N}(i,i+1)$ connectivities. Also shown are the long stretches of $d_{NN}(i,i+1)$ connectivities described above and shown in Figure 1 which are indicative of α-helix in both peptides. These conclusions were supported by several $d_{\alpha N}$-

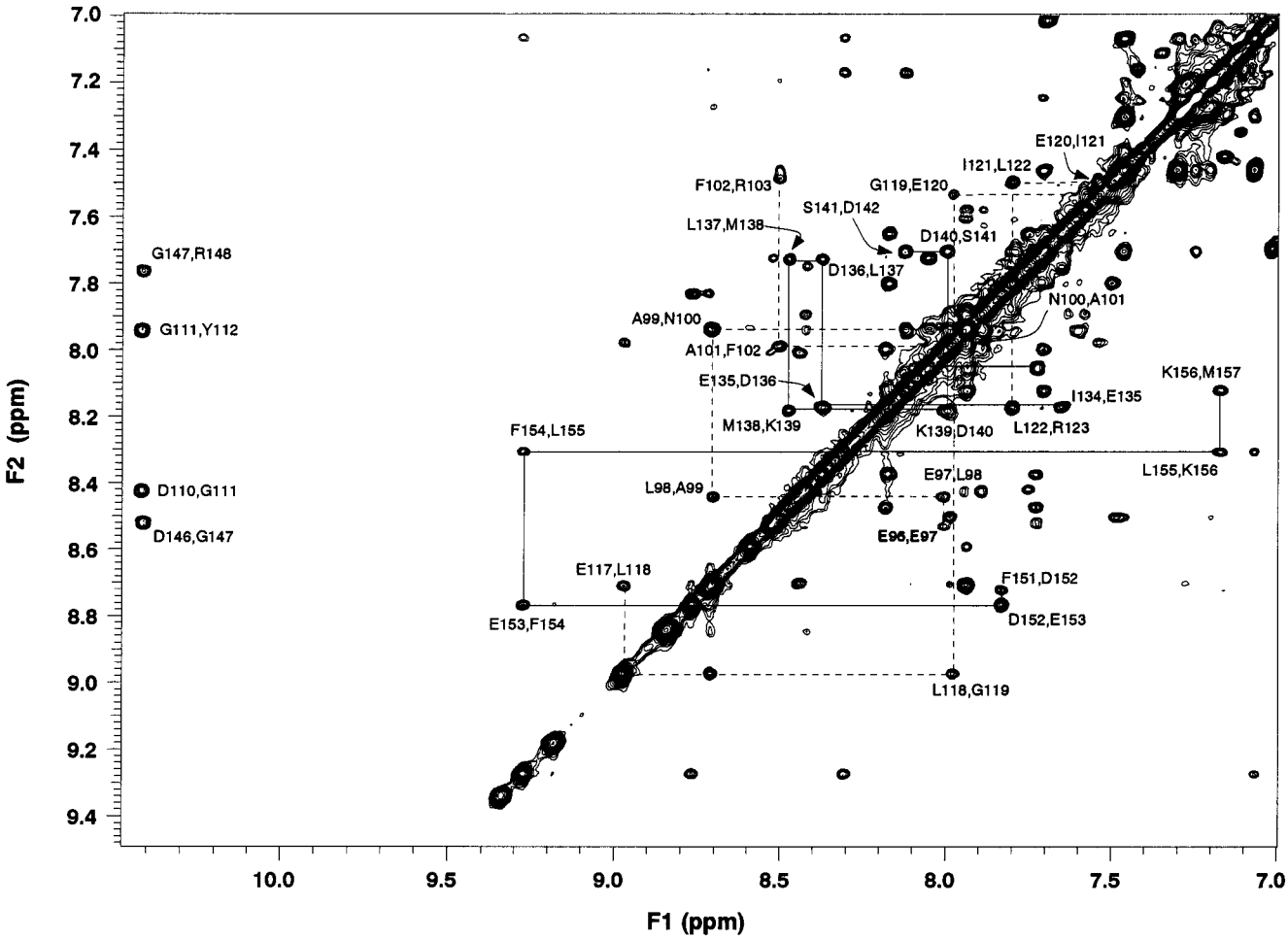

FIGURE 1: Contour plot for the NH/NH region of the 150 ms ^{1}H NOESY spectrum of 2.2 mM SCIII/SCIV acquired at 600 MHz in 90% H_2O/10% D_2O, 6 mM $CaCl_2$, and 100 mM KCl, pH 7.2, and 30 °C. The spectrum shows four stretches of NH/NH connectivities associated with the four α-helices in the SCIII/SCIV heterodimer. Connectivities for the SCIII helices (- - -) and SCIV helices (—) are indicated for residues E96−R103 and E117−R123 in SCIII and I134−D142 and F151−M157 in SCIV. Four cross peaks are also observed (extreme left of plot) corresponding to NH/NH interactions between D110−G111, G111−Y112 in SCIII and D146,G147 and G147,R148 in SCIV.

(i,i+3) and $d_{\alpha\beta}$(i,i+3) interactions between residues E95−D106, D114−R123, E131−D142, and D150−V161. Similar observations have been made in ^{1}H NMR studies of the SCIII homodimer (Shaw et al., 1992b) and a site IV (Kay et al., 1991) homodimer from TnC. In SCIII/SCIV, these regions of α-helix are also in excellent agreement with those in the recently determined NMR structure of calcium-saturated TnC in solution (Slupsky et al., 1995; Slupsky & Sykes, 1995).

The chemical shift index (Wishart et al., 1992) was applied to each residue for its αCH chemical shift to define regions of α-helix and β-sheet in SCIII and SCIV. This analysis agreed well with the NOE data for α-helix location and further suggested that a three-residue β-strand exists in each peptide at residues Y112−D114 (SCIII) and R148−D150 (SCIV). The latter proposal was supported by strong $d_{\alpha N}$(i,i+1) NOEs between Y112−D114 and R148−I149, nearly unobservable intraresidue $d_{HN\alpha}$ NOEs, and large $^3J_{HN\alpha}$ coupling constants (9−12 Hz) for these residues. The αCH chemical shifts of these residues are also remarkably similar (average $\Delta\delta$ 0.07 ppm for six residues) for those found in calcium-saturated TnC where a β-sheet is present (Slupsky et al., 1995). Together, these observations suggest that SCIII is comprised of two α-helices between residues E95−D106 and E116−R123 and a short β-strand between Y112 and D114. Peptide SCIV is comprised of α-helices stretching from residues E131−D142 and F151−E159 with a β-strand between R148 and D150. This initial result, which suggests that 41 residues are in an α-helical conformation, is slightly larger than previous circular dichroism studies which propose SCIII/SCIV contains approximately 34 α-helical residues (Shaw et al., 1994). Upon examination of the DGII structures (below) regular helices for 36 residues, encompassing E97−F105, I115−R123, E132−D140, and F151−E159, were identified in agreement with the CD data.

Heterodimer Formation. The sequential assignment of the SCIII/SCIV heterodimer shows that both peptides are folded but yields little information about the tertiary fold in this synthetic protein domain. In particular, while it is clear that each peptide forms a helix−loop−helix calcium-binding motif, it is not obvious that the two peptides interact in solution. The identification of a β-strand in both SCIII (Y112−D114) and SCIV (R148−D150) was the first evidence of an association between the two peptides where each peptide would provide one-half of the β-sheet. Previous studies (Slupsky et al., 1992) have further shown that several long-range NOEs exist between aromatic protons of F102 in SCIII and both F151 and F154 in SCIV, confirming that the two peptides are packed together in this region. In the analysis of the NOESY data, many other long-range NOEs were observed which provide evidence for heterodimer formation. Figure 3 shows a region of the 150 ms NOESY spectrum which contains NOEs between the aromatic protons

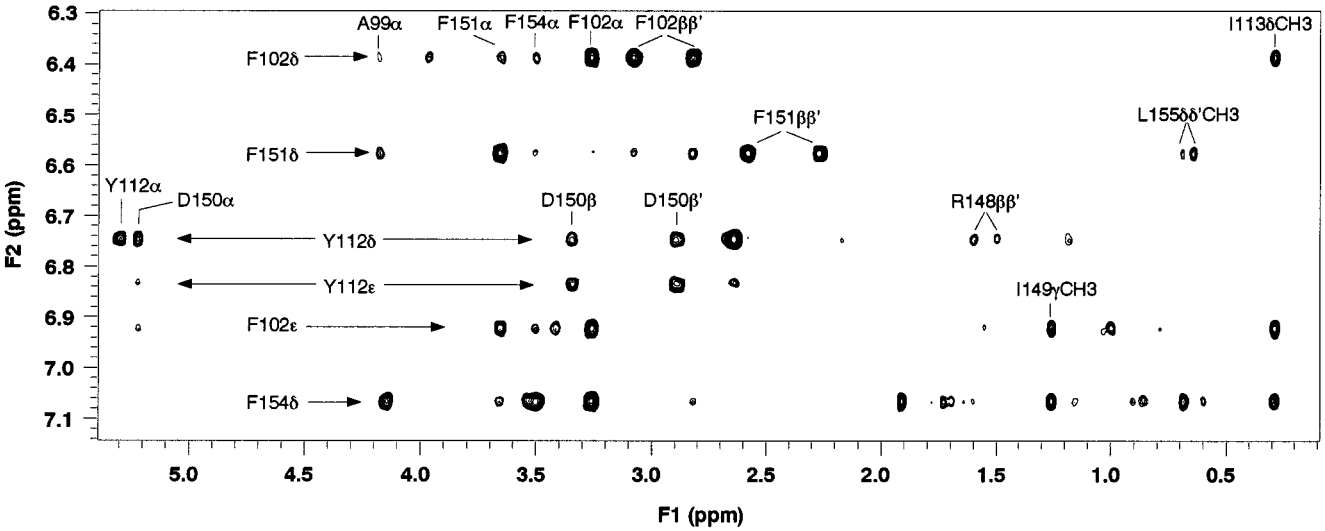

FIGURE 2: Summary of the sequential NOE connectivities and backbone coupling constants ($^3J_{HN\alpha}$) for the Ca_2-SCIII/SCIV heterodimer. The amino acid sequence and residue numbers are shown at the top of the figure. The $d_{\alpha N}$, d_{NN}, and $d_{\beta N}$ are classified by the NOE volume (strong, medium, or weak) measured from the 75 ms NOESY spectrum in 90% H_2O/10% D_2O at 30 °C. The $d_{\alpha N(i,i+3)}$ and $d_{\alpha\beta(i,i+3)}$ connectivities are shown if a cross peak was observed in the 150 ms mixing time NOESY spectrum in D_2O. Dashed lines indicate that the cross peak may be present but overlaps with other cross peaks. Backbone coupling constants are shown as boxes and reflect the relative size of the coupling where (●) is $^3J_{HN\alpha} < 6$ Hz and (□) is $^3J_{HN\alpha} > 10$ Hz for peaks that could be unambiguously measured in DQF-COSY spectra. Differences in chemical shift between the observed and random coil values ($\delta_{obs} - \delta_{rc}$) for αCH (Wishart et al., 1991) are shown as bars. The bottom of the figure shows the secondary structure of Ca_2-SCIII/SCIV interpreted from this data.

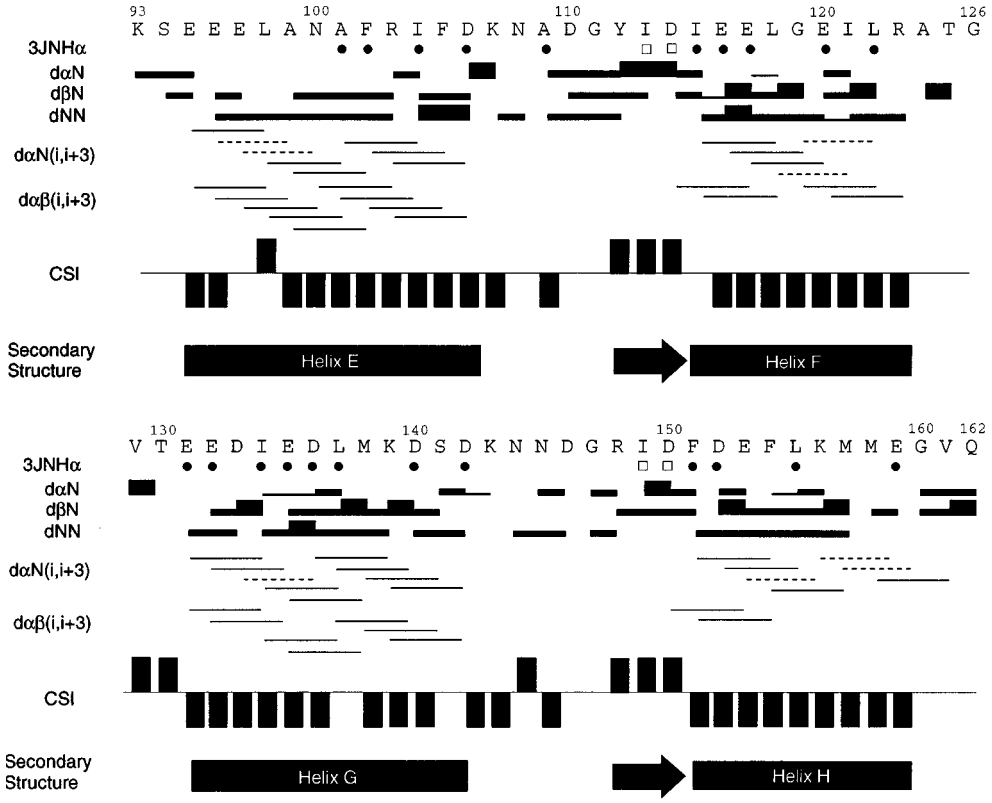

FIGURE 3: Portion of a contour plot showing the aromatic−aliphatic region of of the 150 ms ^1H NOESY spectrum of 2.2 mM SCIII/SCIV acquired at 600 MHz in 99.6% D_2O, 6 mM $CaCl_2$, and 100 mM KCl, pH 7.2, and 30 °C. The spectrum shows NOEs associated with several of the aromatic residues in the SCIII/SCIV heterodimer. Indicated in the figure are several NOEs involving (F_2, top to bottom) F102δ, F151δ, Y112δ, Y112ϵ, F102ϵ, and F154δ from SCIII (F102, Y112) and SCIV (F151, F154) with other residues in both peptides (along F_1). The figure shows many NOEs involving one residue in the SCIII sequence and another in SCIV.

of F102 and Y112 in SCIII and F151 and F154 in SCIV. Several of the assigned NOEs correspond to intraresidue interactions. Also included in these data are long-range NOEs involving residues on each of the two peptides; F102 and F151, A99 and F151, A99 and F154, I113 and F154, and Y112 and D150. A summary of these contacts is illustrated in Figure 4A. These data clearly show that hydrophobic residues on the E-helix of site III (A99, F102) are packed with hydrophobic residues on the H-helix of site IV peptide (F151, F154).

The analysis of long-range interactions involving aromatic residues was more facile due to the excellent spectral

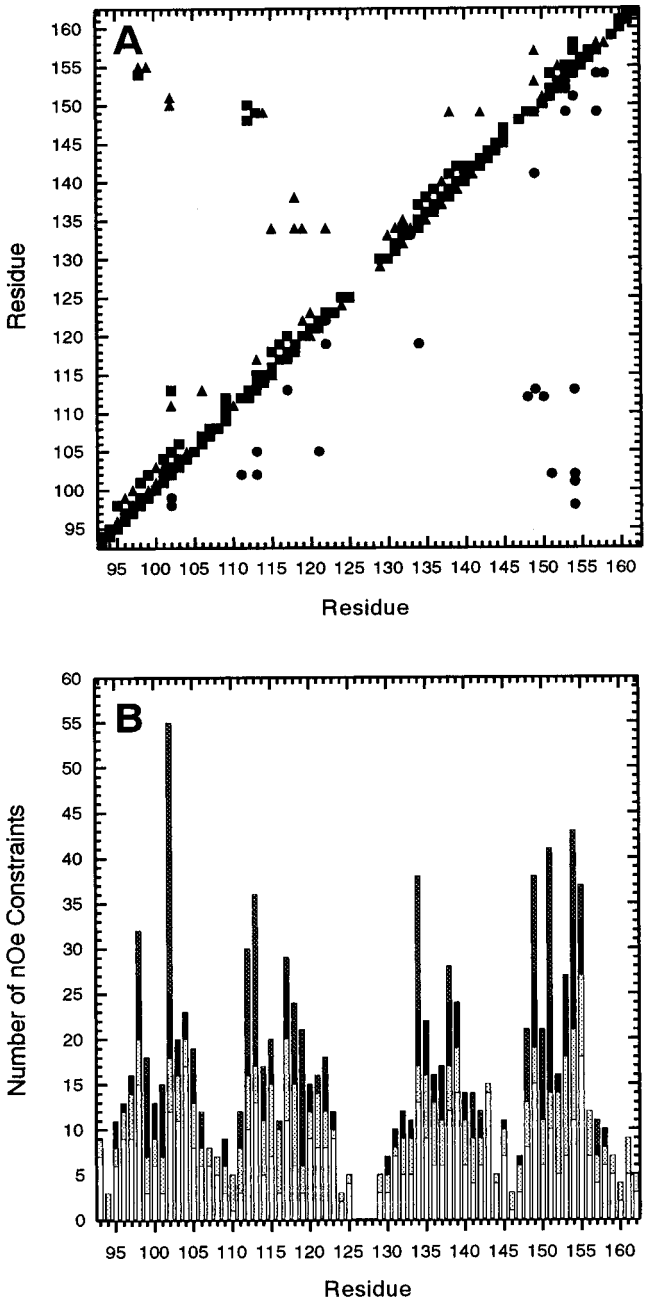

FIGURE 4: Summaries of NOEs observed and type of interaction for the SCIII/SCIV heterodimer. (A) Diagonal plot of the observed NOEs for the SCIII/SCIV heterodimer based on the peptide sequence. Indicated are the observed NOEs (τ_{mix} = 50 ms) between residue pairs of backbone protons (■), backbone−side chain residue pairs (▲), and side chain−side chain residue pairs (●). (B) Histogram of the number of NOE distance constraints determined per residue for the SCIII/SCIV heterodimer based on observed NOEs in the 50 ms NOESY spectrum In this figure all NOEs are indicated twice to reflect the two residues involved in the NOE. The four types of bars indicate intraresidue (open bars), sequential, (light stippled bars), medium-range, (solid bars), and long-range contacts (darkly stippled bars).

dispersion of the aromatic protons in F102, F151, and F154. For long-range interactions between aliphatic side chains, particularly in the F-helix and G-helix, this analysis was more difficult due to significant peak overlap in these regions. Nevertheless, several unambiguous interactions between SCIII and SCIV were observed including G119 αα′ in SCIII with I134 βCH, γCH, γCH_3 and δCH_3 in SCIV and L118 δCH_3 and L122 δCH_3 in SCIII with I134 αCH in SCIV (Figure 4A). Like the above analysis of aromatic NOEs, this pattern of NOEs suggests packing of the F-helix of SCIII with the G-helix in SCIV and that the residues involved are primarily hydrophobic.

Tertiary Structure of SCIII/SCIV. The solution structure of the heterodimer was determined from a set of 646 measured NOEs, comprised of 416 intraresidue and 230 interresidue contacts. Of this latter group, 117 NOEs were sequential ($i-j = 1$), 56 were medium range ($2 \leq i-j \leq 4$), and 62 were long range ($i-j \geq 5$) including 47 interpeptide NOEs. A plot of these intra- and interresidue contacts (Figure 4A) reveals long-range contacts between helix E and helix H and between helix F and helix G in the two peptides. Of particular interest in this figure was the observation of side chain−side chain interactions between Y112, R148, and D150, and I113 with I149 (closed circles, lower right) which indicate interactions across the short three-residue β-sheet between the two peptides. Figure 4B summarizes the total number of distance constraints derived from measured NOEs on a per residue basis. This figure clearly illustrates that the greatest number of NOEs involve the hydrophobic residues L98, F102, I113, I134, I149, F151, F154, and L155.

Distance geometry calculations (DGII), performed for a total of 50 structures, provided 42 structures which converged to an error function of <0.3, and which could be superimposed pairwise to determine a consistent three-dimensional fold for the dimer. An analysis of all 42 structures (Laskowski et al., 1993) indicated that 77.9% of the residues fell within the most favored regions of the Ramachandran plot. Figure 5A shows the superposition of these 42 structures using the four regions E97−F105, D114−R123, E132−D140, and F151−E159. A ribbon diagram of the average structure of the SCIII/SCIV heterodimer is shown in Figure 5B. The structure of the SCIII/SCIV heterodimer consists of four well-defined α-helices as predicted from Figure 2. It is evident from Figure 6, where the RMS deviation on a per residue basis is plotted, that these α-helical regions which encompass residues E97−F105, D114−R123, E132−D140, and F151−E159 have the lowest backbone RMS deviation in the dimer. In addition, this figure shows that the N-termini of helices E and G and the C-termini of helices F and H become unstructured as judged by their large RMS values. These observations are similar to those found for other TnC peptide dimers (Kay et al., 1991; Shaw et al., 1992b), calbindin D_{9k} (Akke et al., 1992; Kordel et al., 1993), and the N-terminal domain of TnC (Findlay et al., 1994). In SCIII/SCIV two helices are present in each peptide with an intervening calcium-binding site to yield the helix−loop−helix motif. The helices in SCIII (E,F) and SCIV (G,H) have interhelical angles of about 102° and 118°, respectively, well within the range for similar pairs of helices in other calcium-binding sites (Strynadka & James, 1989). This allows the inner face of helices E and F on the SCIII peptide to interact with the inner surfaces of helices G and H respectively on SCIV. As is observed in the x-ray structures of troponin C (Herzberg & James, 1988; Satyshur et al., 1988, 1994), this allows for a significant clustering of hydrophobic residues at the interface of the two calcium-binding sites. In particular, in SCIII/SCIV the residues involved are L98, A99, F102, Y112, I113, L118, and G119 in SCIII and I134, M138, R148, I149, F151, F154, and L155 in SCIV. A short antiparallel β-sheet is present at the interface of SCIII/SCIV which is comprised of residues Y112−D114 from SCIII and

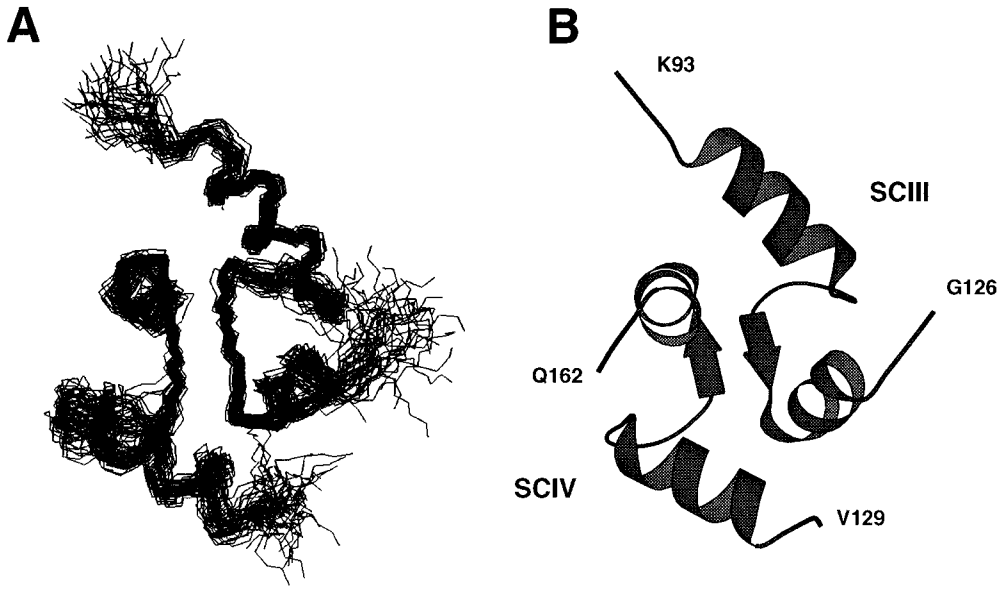

FIGURE 5: (A) Superposition of the 42 DGII structures for the SCIII/SCIV heterodimer. The structures were superimposed on the average structure for residues E97−F105, D114−R123, E132−D140, and F151−E159 for the backbone atoms (N, Cα, C). Residues G160−Q162 show no regular structure and are not displayed for clarity. (B) Average structure for the SCIII/SCIV heterodimer calculated from the backbone atom coordinates of all residues after 250 steps of steepest descents energy minimization. The resulting structure displays 88.3% of all residues in the most allowed regions of the Ramachandran plot and a further 8.3% in allowed regions as determined using the program PROCHECK (Laskowski et al., 1993). The structure is displayed using the program MOLSCRIPT (Kraulis, 1991) in the same orientation as the structures shown in panel A.

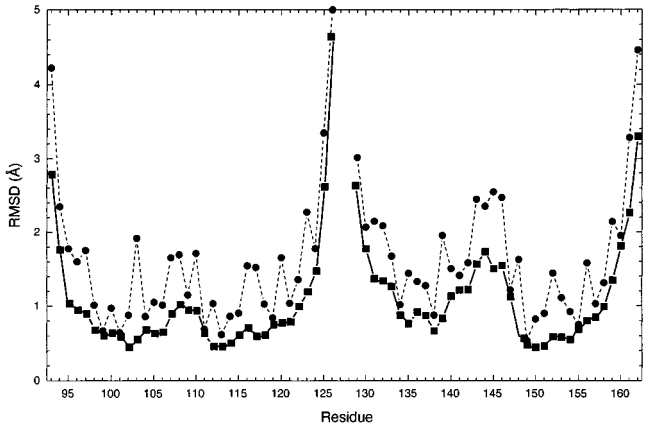

FIGURE 6: Atomic rms deviations per residue for the 42 DGII structures for the SCIII/SCIV heterodimer. The plot shows the pairwise RMSD about the average structure for the backbone (N, Cα, and C) atoms (■) and for all heavy atoms (●). In each case the individual DGII structures were superimposed with the average structure for all residues in the SCIII/SCIV sequence.

R148−D150 from SCIV. In this configuration the side chains of residues Y112−D150, I113−I149, and D114-R148 are close in space in agreement with several long-range NOEs observed between these pairs of residues (Figure 4A).

The superposition of regions E97−F105, D114−R123, E132−D140, and F151−E159, yielded a RMSD of 0.86 ± 0.17 Å between the individual structures and the average structure for backbone atoms (Table 1). From this comparison it is evident that some deviation from the average structure is apparent leading to a significant standard deviation (0.17 Å) from the mean. To determine which region of the SCIII/SCIV heterodimer contributed most to this, a superposition of pairs of helices was done. The results in Table 1 show that individually the helices are nicely defined having an average RMSD of about 0.27 Å. However, when the helices are compared as pairs or triads, it becomes evident that the relationship of the helices differs somewhat. For example, the RMS deviation for the site III regions (E97−F105 and D114−R123) is 0.52 Å and is substantially different from that for site IV (0.78 Å, E132−D140 and F151−E159). Similar trends are noted for all comparisons involving E132−D140 and one or more other region, even though the RMS for region E132−D140 (0.31 Å) is second lowest among the helices. These observations suggest that some uncertainty in the position of helix G with respect to the other three helices in the SCIII/SCIV heterodimer exists. This likely arises from a deficiency of long-range NOEs involving protons in helix G, where the lowest density of this NOE type was noted when compared to the other three helices (Figure 4B).

Figures 5 and 6 show that the calcium-binding loops are as well defined as the helices when superimposed together. However, when the four helical regions are superimposed (Figure 5A), a significant amount of disorder is present in the first five residues of each calcium binding loop (Figure 6). Figure 4B shows that this may be a result of a lack of NOE constraints in these regions of the loop, an observation which is very similar to that found in the N-terminal domain of TnC and in calbindin D_{9k}. In the case of calbindin D_{9k}, this disorder is a result of a lack of NOE data rather than flexibility since ^{15}N relaxation studies show these loops are about as rigid as the α-helical regions (Kordel et al., 1992). A similar situation may be occurring in the SCIII/SCIV heterodimer.

A comparison was made between the SCIII/SCIV heterodimer with the C-terminal domain of TnC (Table 1). From this it is clear that the individual E, G, and H helices in SCIII/SCIV are very similar to those in TnC, having an average RMSD of 0.34 Å. Helix F is less similar to its counterpart in TnC (RMSD = 0.60 Å). When comparing all four helices together the RMSD between the two structures is about 1.40 Å, a value quite similar to that obtained for the SCIII homodimer (1.64 Å). The most significant differences

Table 1: Structural Characteristics of the SCIII/SCIV Heterodimer

Residual Violations	
distance range	average no. of violations
$0.1 \leq d \leq 0.2$	0.36
$0.2 \leq d$	1.60
maximum distance violation	0.46
dihedral > 1°	0.67

Structural Deviations		
	atomic RMS deviation (Å)	
regions	backbone (C, Cα, N)	all heavy atoms
all helices[a]	0.86 ± 0.17	1.54 ± 0.15
E97−F105, D114−R123	0.52 ± 0.12	1.40 ± 0.11
E132D140, F151−E159	0.78 ± 0.20	1.46 ± 0.17
E97−F105, F151−E159	0.41 ± 0.08	1.25 ± 0.08
D114−R123, E132−D140	0.70 ± 0.12	1.50 ± 0.14
E97−F105, D114−R123, F151−E159	0.65 ± 0.14	1.41 ± 0.10
E97−F105, E132−D140, F151−E159	0.77 ± 0.17	1.47 ± 0.15
E97−F105	0.20 ± 0.03	1.19 ± 0.12
D114−R123	0.38 ± 0.08	1.31 ± 0.09
E132−D140	0.31 ± 0.05	1.26 ± 0.15
F151−E159	0.38 ± 0.09	1.17 ± 0.08
calcium-binding loops[b]	0.93 ± 0.17	1.63 ± 0.19
D106−E117	0.57 ± 0.14	1.31 ± 0.17
D142−E153	0.97 ± 0.20‘	1.75 ± 0.28
vs TnC X-ray[c]		
all helices[a]	1.40	
helices[d]	0.38, 0.60, 0.27, 0.37	
calcium-binding loops[b]	1.41	

[a] Helices are defined as E97−F105, D114−R123, E132−D140, and F151−E159. [b] Calcium-binding loops in SCIII/SCIV are D106−E117 and D142−E153. [c] Compared to the X-ray structure of turkey skeletal troponin C. [d] Individual helices listed in order shown in (d).

between the average SCIII/SCIV heterodimer structure and that of TnC are the interhelical angles and distances between helices at the dimer interface. In the SCIII/SCIV heterodimer structures the interhelical angles for the E/H and F/G helices are about 99° and 121°, respectively, compared to 116.4° and 124.7° in the X-ray structure of turkey skeletal TnC (Herzberg & James, 1988). In TnC the interhelical distance for helices E and H is about 10.8 Å compared to 11.7 Å in the SCIII/SCIV heterodimer structures. This observation is magnified when helices F and G are compared. In TnC this interhelical distance is about 10.5 Å compared to 12.0 Å in the SCIII/SCIV heterodimer. These observations indicate that subtle differences may exist between the solution and crystal forms of the C-terminal domain.

In the SCIII/SCIV heterodimer the position of the G helix is less well defined with respect to the other three helices. This observation appears to be a recurring theme in several solution structures of EF-hand calcium-binding proteins. In TR_1C the C-helix, which is analogous to the G-helix in the C-terminal domain, exhibits significant mobility (Findlay et al., 1994). In recoverin, helix D has been found to be conformationally flexible in solution as have the C and G helices in apo-calmodulin (Kuboniwa et al., 1995; Zhang et al., 1995). These observations suggest that the packing of the B/C and F/G helix pairs in TnC and calmodulin and helix D with helices E and F in recoverin is poorer than the packing of other helix pairs in these proteins. It is interesting that in TnC and calmodulin, both helices C and G possess no aromatic residues and pack with helices (B or F) which also lack aromatic residues. Conversely, the helix pairs A/D and E/H in these two proteins each have several phenylalanine residues which interact at the helix−helix interface. Based on the observations from the SCIII/SCIV heterodimer, TR_1C, and calmodulin, this may suggest that the phenylalanine packing for the A/D and E/H helix pairs is the most important contribution toward the stability of these two-site domains.

Structural Comparisons with TnC and the SCIII Homodimer. Several three dimensional structures of the C-terminal domain of TnC are available including X-ray structures of TnC (Herzberg & James, 1988; Satyshur et al., 1988; Satyshur et al., 1994) and solution NMR structures of TnC (Slupsky & Sykes, 1995) and the SCIII homodimer (Shaw et al., 1992b). A comparison of the SCIII/SCIV heterodimer with these structures reveals that the global folds of these structures are all quite similar having a maximum RMSD of about 1.64 Å for the four defined helices.

The interhelical angles and distances for the TnC structures were also compared (Table 2). These structural properties can be subject to variability between the individual NMR structures, the methods of calculation for both the structures and their geometries, and the residues used for the calculations. In order to assess the structural variability between NMR structures, we chose to use the ensemble of calculated structures rather than an average solution structure for SCIII/SCIV or TnC. This allows a standard deviation to be calculated from the mean, providing some measure of the differences between structures. We also recalculated the SCIII/SCIV structure using the X-PLOR protocol (30 structures) to assess the method of calculation on the measured angles and distances and compare the results to the DGII derived structures. Further, residues used for geometry calculations were those defined for the four helices in SCIII/SCIV (Table 1) to minimize a selection factor in the calculation. Taking these factors into account, our comparison of the C-terminal domain structures show that the intrasite E/F and G/H angles for the SCIII/SCIV heterodimer are very similar (102° and 118°, respectively) to that observed for the X-ray TnC structure (Herxberg &

Table 2: Interhelical Angles/Distances in TnC C-Terminal Domain Structures

helix pair	SCIII/SCIV DGII[a]	SCIII/SCIV X-PLOR[b]	solution TnC NMR[c]	TnC X-ray[d]	SCIII/SCIII[e]
angle					
E/F	102 ± 5	102 ± 6	90 ± 5	108.4	113.5
G/H	118 ± 10	118 ± 8	117 ± 6	113.8	119.7
E/H	99 ± 5	109 ± 5	103 ± 5	116.4	88.2
F/G	121 ± 10	127 ± 12	135 ± 6	124.7	94.5
distance					
E/H	11.7 ± 0.2	11.1 ± 0.3	10.3 ± 0.2	10.8	10.4
F/G	12.0 ± 0.5	11.8 ± 0.6	11.6 ± 0.3	10.5	10.4

[a] This work. [b] Shaw and Sykes (unpublished results). [c] Slupsky and Sykes (1995). [d] Herzberg and James (1988). [e] Shaw et al. (1992a).

James, 1988). The E/F angle for the solution structure of TnC appears to be a bit smaller (90°) than in the other structures. This results in a more open conformation of the C-terminal domain which may be a result of the influence of trifluoroethanol on the structure (C. M. Slupsky, personal communication). Interestingly, it also appears that the SCIII homodimer has adopted angles (114°, 120°) closer to that for site IV in the C-terminal domain than site III. These findings provide a hint of subtle differences between the structures. However, the large range of angles (10−20°) for the solution structures precludes further examination.

In contrast to the intrasite interhelical angles, the intersite interhelical angles show some measurable differences (Table 2). For example, the E/H and F/G angles in the SCIII/SCIV heterodimer are very similar to those observed for the solution and X-ray structures of TnC. However, in the SCIII homodimer both the E/H and F/G interhelical angles are significantly smaller (∼30°) than those observed in the TnC structures or the SCIII/SCIV heterodimer. This latter observation is likely a result of the different packing of the hydrophobic residues at the helix crossing points in the SCIII structure (Shaw et al., 1992b).

As descibed earlier, it has been observed that some conformational flexibility exists for some helices with respect to others resulting in tighter or looser packing of these helices in several calcium-binding proteins . As shown in Table 2 it is clear that both the E/H and F/G helix pairs have larger interhelical distances in solution than in the X-ray structure. In particular the F/G helix pair in the III/IV structure and solution TnC structure is approximately 1.4 Å farther apart compared to the X-ray structure. The interhelical distance for the E/H helix pair is slightly greater (0.3 Å) in the SCIII/SCIV dimer compared to the X-ray structure. These observations were also confirmed from SCIII/SCIV structures determined using X-PLOR suggesting that the distances are not simply a result of the type of calculation used. Rather, the range of distances observed in the SCIII/SCIV structure appear to be a result of mobility of at least one of these helices. As described earlier helix G appears to be the most likely candidate based on superposition of the helices. In addition, the F/G helix pair pack significantly closer in the X-ray structure of TnC than in the solution structures. One interpretation of this observation is that the solution structures reflect a range the mobility of the protein with a range of interhelical distances. In the X-ray structure the hydrophobic component is more important due to a lower dielectric constant in the solid, and the crystal lattice restricts motion thus biasing the X-ray structure toward the shortest of the distances observed in the NMR structures.

Significance of the SCIII/SCIV Dimer Solution Structure. During muscle contraction it has been shown that the C-terminal domain of TnC interacts with the inhibitory region of troponin I (Grabarek et al., 1981). This interaction has been probed by ^{1}H NMR spectroscopy for the SCIII homodimer (Shaw and Sykes, unpublished results), SCIII/SCIV heterodimer, and TnC (Slupsky et al., 1992). It is clear that this must require some mobility of both the C-terminal domain and TnI to facilitate the interaction. Our observations here of a looser C-terminal domain in solution compared to the crystalline state support this idea.

The SCIII/SCIV heterodimer is able to interact with TnIp, while the SCIII homodimer displays a much weaker interaction. Initially, this observation may be surprising since the residues most affected by TnIp binding are I104, Y112, and I121, which are all located in site III. While the analysis of interhelical angles and distances provides some rationale for this difference in interaction of these two dimers with TnIp, it is the exposed surface area displayed by each of the two dimers which is the key factor. As it has been observed that hydrophobic residues (I104, T112, and I121) are affected by the interaction (Slupsky et al., 1992), the hydrophobic surface areas were measured for the solution structures of the SCIII/SCIV and SCIII dimers and TnC. This analysis showed that the accessible surface area for the hydrophobic residues are nearly identical for these three species (1194 ± 45 Å^2). However, in the SCIII/SCIV heterodimer and TnC the contribution from exposed surface area of site III hydrophobes (800 and 740 Å^2, respectively) is about 60% higher than in site IV (470 and 500 Å^2, respectively). As a result the hydrophobic surface area for each site III component in the SCIII dimer is intermediate (∼570 Å^2) to that observed for sites III and IV in the SCIII/SCIV heterodimer and TnC. This shows that the SCIII homodimer has adapted its structure in order to form a stabile dimer and maintain the same amount of buried (or exposed) hydrophobic surface area in the dimer. This may account for the stablility of the SCIII homodimer being very near that of the SCIII/SCIV heterodimer. However, the surface area calculations also provide an explanation for the preferred interaction of TnI with TnC and the SCIII/SCIV heterodimer compared to the SCIII homodimer. Close analysis of these data shows that residues I104, Y112, and I121 are more exposed in the SCIII/SCIV heterodimer, by 14%, 35% and 50%, respectively, compared to the SCIII homodimer. In the SCIII/SCIV heterodimer this greater exposure of these key residues allows for their interaction with TnI as observed in ^{1}H NMR experiments (Slupsky et al., 1992).

The present results provide a picture of the C-terminal domain of TnC being a more mobile, less compact domain in solution than observed in the crystal state. This may facillitate its interaction with TnI. In addition residues I104, Y112, and I121 are more exposed in this domain than in a

symmetric domain comprised of two site III peptides. It is interesting that many multisite calcium-binding proteins are believed to have evolved through gene duplication from a single site. In TnC, an initial two-site domain might have corresponded to a site III homodimer which evolved to its present site III/IV composition. Although very similar in structure, these domains display some different interhelical angles and degrees of exposure of surface hydrophobic residues. The inability for the III/III homodimer to interact with TnIp may suggest that nature has modified the original gene duplicated domain to its present functional two site domain.

ACKNOWLEDGMENT

We thank Robert Boyko and Tim Jellard (University of Alberta) for their invaluable computing assistance and Frank Sönnichsen (University of Alberta) for his help and useful suggestions with DGII calculations. We also thank Kathryn Barber (University of Western Ontario) for her careful measurement of NOE intensity data.

SUPPORTING INFORMATION AVAILABLE

One table listing ^{1}H chemical shift data for the SCIII/SCIV heterodimer (3 pages). Ordering information is given on any current masthead page.

REFERENCES

Akke, M., Drakenberg, T., & Chazin, W. (1992) *Biochemistry 31*, 1011−1020.
Babu, Y. S., Bugg, C. E., & Cook, W. J. (1988) *J. Mol. Biol. 203*, 191−204.
Bax, A., & Davis, D. G. (1985) *J. Magn. Reson. 65*, 355−360.
Declercq, J. P., Tinant, B., Parello, J., Etienne, G., & Huber, R. (1988) *J. Mol. Biol. 202*, 349−353.
Durussel, I., Luan-Rilliet, Y., Petrova, T., Takagi, T., & Cox, J. A. (1993) *Biochemistry 32*, 2394−2400.
Findlay, W. A., Sonnichsen, F. D., & Sykes, B. D. (1994) *J. Biol. Chem. 269*, 6773−6778.
Finn, B. E., Kördel, J., Thulin, E., Sellers, P., & Forsén, S. (1992) *FEBS Lett. 298*, 211−214.
Flaherty, K. M., Zozulya, S., Stryer, L., & McKay, D. B. (1993) *Cell 75*, 709−716.
Grabarek, Z., Drabakowski, W., Leavis, P. C., Rosenfeld, S. S., & Gergely, J. (1981) *J. Biol. Chem. 256*, 13121−13127.
Herzberg, O., & James, M. N. G. (1988) *J. Mol. Biol. 203*, 761−779.
Hyberts, S. G., Goldberg, M. S., Havel, T. F., & Wagner, G. (1992) *Protein Sci. 1*, 736−751.
Kay, L. E., Forman-Kay, J. D., McCubbin, W. D., & Kay, C. M. (1991) *Biochemistry 30*, 4323−4333.
Kline, A. D., Braun, W., & Wüthrich, K. (1988) *J. Mol. Biol. 204*, 675−724.
Kordel, J., Skelton, N. J., Akke, M., Palmer, A. G., & Chazin, W. J. (1992) *Biochemistry 31*, 4856−4866.
Kordel, J., Skelton, N. J., Akke, M., & Chazin, W. J. (1993) *J. Mol. Biol. 231*, 711−734.
Kraulis, P. J. (1991) *J. Appl. Crystallogr. 24*, 946−950.
Kretsinger, R. H., & Nockolds, C. E. (1973) *J. Biol. Chem. 248*, 3313−3326.
Kuboniwa, H., Tjandra, N., Grzesiek, S., Ren, H., Klee, C. B., & Bax, A. (1995) *Nature Struct. Biol. 2*, 768−776.
Laskowski, R. A., MacArthur, M. W., Moss, D. S., & Thornton, J. M. (1993) *J. Appl. Crystallogr. 26*, 283−291.
Linse, S., Thulin, E., & Sellers, P. (1993) *Protein Sci. 2*, 985−1000.
Marsden, B. J., Shaw, G. S., & Sykes, B. D. (1989) *Biochem. Cell Biol. 68*, 587−601.
Monera, O. D., Shaw, G. S., Zhu, B.-Y., Sykes, B. D., Kay, C. M., & Hodges, R. S. (1992) *Protein Sci. 1*, 945−955.
Piantini, U., Sorensen, O. W., & Ernst, R. R. (1982) *J. Am. Chem. Soc. 104*, 6800−6801.
Satyshur, K. A., Rao, S. T., Pyzalska, D., Drendel, W., Greaser, M., & Sundaralingam, M. (1988) *J. Biol. Chem. 263*, 1628−1647.
Satyshur, K. A., Pyzalska, D., Greaser, M., Rao, S. T., & Sundaralingam, M. (1994) *Acta Crystallogr. D 50*, 40−49.
Shaw, G. S., Hodges, R. S., & Sykes, B. D. (1990) *Science 249*, 280−283.
Shaw, G. S., Hodges, R. S., & Sykes, B. D. (1991a) *Biochemistry 30*, 8339−8347.
Shaw, G. S., Golden, L. F., Hodges, R. S., & Sykes, B. D. (1991b) *J. Am. Chem. Soc. 113*, 5557−5563.
Shaw, G. S., Findlay, W. A., Semchuk, P. D., Hodges, R. S., & Sykes, B. D. (1992a) *J. Am. Chem. Soc. 114*, 6258−6259.
Shaw, G. S., Hodges, R. S., & Sykes, B. D. (1992b) *Biochemistry 31*, 9572−9580.
Shaw, G. S., Hodges, R. S., & Sykes, B. D. (1992c) *Biopolymers 32*, 391−397.
Shaw, G. S., Hodges, R. S., Kay, C. M., & Sykes, B. D. (1994) *Protein Sci. 3*, 1010−1019.
Slupsky, C. M., & Sykes, B. D. (1995) *Biochemistry 34*, 15953−15964.
Slupsky, C. M., Shaw, G. S., Campbell, A. P., & Sykes, B. D. (1992) *Protein Sci. 1*, 1595−1603.
Slupsky, C. M., Reinach, F. C., Smillie, L. B., & Sykes, B. D. (1995) *Protein Sci. 4*, 1279−1290.
States, D. J., Haberkorn, R. A., & Rubin, D. J. (1982) *J. Magon. Reson. 48*, 286−292.
Strynadka, N. C. J., & James, M. N. G. (1989) *Annu. Rev. Biochem. 58*, 951−998.
Swain, A. L., Kretsinger, R. H., & Amma, E. L. (1989) *J. Biol. Chem. 264*, 16620−16628.
Szebenyi, D. M. E., & Moffat, K. J. (1986) *J. Biol. Chem. 261*, 8761−8777.
Wagner, G., Braun, W., Havel, T. F., Schaumann, T., Go, N., & Wüthrich, K. (1987) *J. Mol. Biol. 196*, 611−639.
Wishart, D. S., Sykes, B. D., & Richards, F. M. (1992) *Biochemistry 31*, 1647−1651.
Wüthrich, K. (1985) *NMR of Proteins and Nucleic Acids*, John Wiley, New York.
Zhang, M., Tanaka, T., & Ikura, M. (1995) *Nature Struct. Biol. 2*, 758−767.

BI9528006